LIGHTWEIGHT ALGORITHMS FOR COLLISION AVOIDANCE APPLICATIONS

Juan Luis Gonzalo [(1)], Camilla Colombo [(1)]

[(1)] Politecnico di Milano, Department of Aerospace Science and Technology, Via La Masa 34, 20158 Milan, Italy, juanluis.gonzalo@polimi.it

ABSTRACT

The flourishing of the new space economy, characterized by new mission types, capabilities, space-based services, and players, is increasing congestion in space, particularly in low Earth orbit. To deal with the growing amount of data and potentially dangerous close approaches, as well as to enable new autonomous capabilities, lightweight and accurate algorithms are required.
This work presents the latest advancements in a suite of algorithms for the modelling and design of collision avoidance manoeuvres (CAMs). First, a fully analytical approximation for low-thrust CAMs is developed, achieving significant improvements in both accuracy and computational time with respect to the previous semi analytical model. Then, a procedure to numerically propagate state transition matrices including the effects of drag and solar radiation pressure is presented. Several numerical test cases are studied to assess the performance of these solutions. Finally, the potential use of these algorithms in combination with machine learning models for autonomous on-board operations is discussed, and a proposed demonstration mission is presented.

1 INTRODUCTION

Low Earth orbit is becoming an increasingly congested region, partly due to the flourishing of a new space economy. Bolstered by cost reductions in hardware and launch services, several companies are proposing and deploying new constellations for diverse space-based services such as communications or Earth monitoring. A significant example is the Starlink space-based-internet constellation by SpaceX, currently composed of 1,684 satellites but approved by the US Federal Communications Commission for more than 12,000. Furthermore, NASA and the US military are actively studying synergies with the private sector, seeking for benefits in terms of cost, deployment times, and robustness. In this increasingly congested scenario, Collision Avoidance (COLA) activities are expected to increase both in frequency and complexity. A recent warning call came on 2 September 2019, when ESA had to manoeuvre its Aeolus winds monitoring spacecraft to avoid a potential Close Approach (CA) with a Starlink satellite. This event underlines the need for improvement not only in tracking capabilities, but also in procedures, communications, and the efficient management of increasingly large sets of data. Among the different strategies to tackle this last issue, the availability of fast algorithms for the analysis of CAs and the design of Collision Avoidance Manoeuvres (CAMs) can prove a very useful tool.
For the last three years, the European Research Council-funded COMPASS project [1] has being developing new approaches and tools for the analysis and design of CAMs, with a focus on computational efficiency. These algorithms rely on analytical and semi analytical methods for the modelling of changes in the orbital elements due to different types of forces, such as impulsive [2][3] or low-thrust [4] CAMs. The changes in orbital elements are mapped into displacements at the

nominal CA through relative motion models, and the resulting displacements are analysed in the b-plane to separate the effects of phase change and geometry change. Different criteria for the optimization of the CAM are considered, mainly maximization of the miss distance and minimization of the collision probability. For fully analytical models the optimization problem can be reduced to an eigenvalue/eigenvector one [5][6], while the high computational efficiency of semi analytical models allows for their use in parametric analyses or in combination with optimisation algorithms. The evolution of uncertainties before the CA has also been considered [7], particularly regarding the contribution of drag and Solar Radiation Pressure (SRP). The models allow for the computation of State Transition Matrices (STMs), which can be used for the propagation of covariances or design of several types of CAMs. Gathering all these developments, the Manoeuvre Intelligence for Space Safety (MISS) software tool was introduced to provide an integrated approach to Space Situational Awareness (SSA)-related operational activities [8]. The high computational efficiency of this tool makes it suitable for several applications, such as on-board and autonomous operations or in combination with Artificial Intelligence (AI) algorithms (e.g., to accelerate training).

This paper presents the latest developments in the underlying algorithms of MISS, with focus on improving computational efficiency and modelling new perturbing forces. The former is achieved through the introduction of new analytical models, to complement or replace previous semi analytical ones. The capabilities for the computation of STMs are also expanded, to better incorporate the effect of perturbations like drag and SRP. Several test cases assessing the accuracy and numerical performance of the models are presented, quantifying the reductions in computational time due to the use of analytical approaches compared to semi analytical and fully numerical ones.

The rest of this manuscript is organized as follows. Section 2 provides a brief overview of the main elements and design philosophy of the algorithms in MISS. A new, fully analytical model for low-thrust CAMs in developed in Section 3, leveraging averaging techniques. The analytical model is pitched against the semi analytical one developed in previous works [4][8][9], to assess its advantages in terms of accuracy and computational cost, and whether it can complement or replace the semi analytical model. Section 3 presents an extension to the STM computation capabilities in PlanODyn. Particularly, by defining an extended state vector including the area-to-mass ratio and the drag and reflectivity coefficients, it is possible to directly apply the resulting STM to the design of CAMs by sails based on the modification of the effective area-to-mass. The discussion is closed in Section 5 with a qualitative analysis of the possible application of these models for autonomous operations in combination with AI and machine learning (ML) techniques, and a proposed demonstrator mission is briefly presented. Finally, conclusions are drawn.

2 CAM MODELLING FRAMEWORK

The algorithms implemented in MISS [2][9] allow to characterize the CA at the Time of Closest Approach (TCA), t_{CA}, between a manoeuvrable spacecraft and a debris, and model different types of CAMs. Depending on the control capabilities of the spacecraft, the algorithms allow for the evaluation of the displacement and change of collision probability for a given CAM profile, or the optimization of the manoeuvre for different figures of merit. In all cases, these algorithms are organized around three main elements [2][9]:

1. Dynamical models for the modification of the orbit, expressed through changes in its vector of Keplerian elements $\boldsymbol{\alpha} = [a, e, i, \Omega, \omega, M]$.
2. Relative motion equations linearized around the nominal orbit of the spacecraft, mapping changes in the Keplerian elements $\delta\boldsymbol{\alpha}$ into changes in state $\delta\boldsymbol{s}$ at the TCA. In matrix form, $\delta\boldsymbol{s}(t_{CA}) = \boldsymbol{A}\ \delta\boldsymbol{\alpha}(t_{CA})$. Matrix $\boldsymbol{A}$ only depends on the nominal orbit, and its expression can be found in [2].

3. Derivation of actionable information for the CAM design process. Particularly, computation of collision probabilities and projection of the manoeuvre in the b-plane of the encounter.

This work focuses on the latest advances for the first element, the modelling of the orbit modification due to the CAM. Particularly, Section 3 presents an analytical model for low-thrust CAMs that replaces the semi analytical solutions in [4][8][9], providing improvements both in accuracy and computational cost. The inclusion of additional perturbations is then dealt with in Section 4, where a method to compute STMs that include the effect of changes in drag and SRP is presented, using the semi analytical, single-averaged orbit propagator PlanODyn [10].

The displacements will be expressed in the b-plane. This is the plane orthogonal to the relative velocity of the spacecraft with respect to the debris at the TCA.

3 ANALYTICAL MODEL for LOW-THRUST CAM

The low-thrust CAM model is developed assuming a constant, tangential thrust control law applied during an arc of duration Δt_{CAM} before the CA. The choice of tangential thrust is based on previous results which show that the optimal thrust orientation tends to align with the tangential direction for lead times longer than a period [3][11]. The evolution of the Keplerian elements of the spacecraft during the thrust arc are given by Gauss planetary equations, particularized for tangential thrust:

$$\begin{aligned} \frac{\mathrm{d}a}{\mathrm{d}t} &= \frac{2a^2 v}{\mu} a_t, & \frac{\mathrm{d}e}{\mathrm{d}t} &= \frac{1}{v} 2(e+\cos f) a_t \\ \frac{\mathrm{d}i}{\mathrm{d}t} &= 0, & \frac{\mathrm{d}\Omega}{\mathrm{d}t} &= 0\,, & \frac{\mathrm{d}\omega}{\mathrm{d}t} &= \frac{1}{ev} 2\sin f\, a_t \\ \frac{\mathrm{d}M}{\mathrm{d}t} &= n - \frac{\sqrt{1-e^2}}{ev} 2\left(1+\frac{e^2 r}{p}\right)\sin f\, a_t, & \frac{\mathrm{d}E}{\mathrm{d}t} &= \frac{na}{r} - \frac{2\sin f}{e\sqrt{1-e^2}\, v}\, a_t \end{aligned} \tag{1}$$

where f is the true anomaly, a_t is the thrust acceleration, μ is Earth's gravitational parameter, n is the mean motion, p is the semilatus rectum of the orbit, and v is its velocity. It is observed that inclination and right ascension of the ascending node remain constant under a purely tangential action. To obtain analytical expressions for the evolution of $\boldsymbol{\alpha}$, in [4][8][9] a change of independent variable is introduced to express the equations in terms of the eccentric anomaly, so that they can be averaged over a period. This change of independent variable is based on the following time law [12]:

$$\frac{\mathrm{d}E}{\mathrm{d}t} \approx \sqrt{\frac{\mu}{a^3}} \frac{1}{1-e\cos E} \tag{2}$$

obtained by taking the derivative with respect to E in Kepler's equation assuming that a and e remain constant. The differential equations for a, e, ω and M finally take the form:

$$\begin{aligned} \frac{\mathrm{d}a}{\mathrm{d}E} &= a_t \frac{2a^3}{\mu}\sqrt{1-e^2\cos^2 E}, & \frac{\mathrm{d}e}{\mathrm{d}E} &= a_t \frac{2a^2(1-e^2)}{\mu}\sqrt{\frac{1-e\cos E}{1+e\cos E}}\cos E \\ \frac{\mathrm{d}\omega}{\mathrm{d}E} &= a_t \frac{2a^2\sqrt{1-e^2}}{\mu e}\sqrt{\frac{1-e\cos E}{1+e\cos E}}\sin E \\ \frac{\mathrm{d}M}{\mathrm{d}E} &= (1-e\cos E)\left(1 - a_t \frac{2a^2(1-e^3\cos E)\sin E}{e\mu\sqrt{1-e^2\cos^2 E}}\right) \end{aligned} \tag{3}$$

In previous works [4][8][9], different semi analytical models based on averaging techniques have been proposed to evaluate $a(E)$, $e(E)$, $\omega(E)$, and $M(E)$ in a computationally efficient way. However, all of them rely on numerical integrations for solving the time law. Particularly, in [4] the equations for semimajor axis and eccentricity were integrated together with the time law in eccentric anomaly for the whole thrust arc, to find the angular position at the final time. Furthermore, to recover the short-periodic oscillations in mean anomaly, its differential equation had to be integrated during the last, incomplete revolution. The performance of the method was improved in [8][9] following the approach proposed by Colombo et al. [13], using a least-squares fitting to approximate the short-periodic terms of semimajor axis and eccentricity as sinusoidal functions. In this way, the solution of the time law for a given final time only required the numerical integration of a single differential equation. However, it is still required to propagate numerically a and e during at least one revolution to perform the fitting (whose coefficients do not depend on initial and final time but do depend on acceleration), and the trigonometric representation chosen only included harmonics of period 2π in the eccentric anomaly.

To address these limitations, this work presents an analytical approximation for the short-periodic terms of a and e. Same as in previous works, the equations of motion are averaged assuming that the slow Keplerian parameters remain constant during one revolution. This assumption is equivalent to consider a small perturbative force. The constant reference values for semimajor axis and eccentricity are named a_{ref} and e_{ref}, respectively. Note that these values will in general be different from the initial ones $a_0 = a(E_0)$ and $e_0 = e(E_0)$. Assuming that a and e remain constant over one revolution and integrating, a solution is found in terms of incomplete elliptic integrals [4][8][9]:

$$a(E) = 2\varepsilon a_{ref}\gamma\ \mathrm{E}[E,m]$$

$$e(E) = 2\varepsilon\frac{\left(1-e_{ref}^2\right)}{e_{ref}}\left(\frac{1}{2}\ln\frac{\sqrt{1-e_{ref}^2\cos^2 E}+e_{ref}\sin E}{\sqrt{1-e_{ref}^2\cos^2 E}-e_{ref}\sin E}-\frac{1}{\gamma}\mathrm{F}[E,m]+\gamma\mathrm{E}[E,m]\right) \tag{4}$$

where $\varepsilon = a_t/\left(\mu/a_{ref}^2\right)$ is a non-dimensional thrust parameter, $\gamma^2 = 1-e_{ref}^2$, $m = -e_{ref}^2/(1-e_{ref}^2)$, and $\mathrm{F}[\cdot,\cdot]$ and $\mathrm{E}[\cdot,\cdot]$ are the incomplete elliptic integral of the first and second kind, respectively. These solutions are exact under the given assumptions; however, they are too cumbersome for further developments such as getting an explicit solution for the time law. To ease their manipulation, we first separate their mean and short-periodic components, in the form:

$$\begin{aligned} a(E) &= a_{ref} + \varepsilon a_{mean}(E) + \varepsilon a_{osc}(E) \\ e(E) &= e_{ref} + \varepsilon e_{mean}(E) + \varepsilon e_{osc}(E) \end{aligned} \tag{5}$$

Through some mathematical manipulations, omitted here for brevity, it is proven that the mean components are linear expressions of the eccentric anomaly:

$$\begin{aligned} a_{mean}(E) &= K_a E, \qquad \text{with}\ \ K_a = \frac{4a_{ref}\ \mathrm{E}[e_{ref}^2]}{\pi} \\ e_{mean}(E) &= K_e E, \qquad \text{with}\ \ K_e = \frac{4\left(1-e_{ref}^2\right)}{e_{ref}\pi}\left(\mathrm{E}\left[e_{ref}^2\right]-\mathrm{F}[e_{ref}^2]\right) \end{aligned} \tag{6}$$

where $\mathrm{F}[\cdot]$ and $\mathrm{E}[\cdot]$ are the complete elliptic integrals of the first and second kind, respectively. Note that $\mathrm{E}\left[e_{ref}^2\right] \in]\pi/2,1]$ for elliptic orbits, while $\mathrm{F}[e_{ref}^2]$ goes to infinity for $e_{ref} \to 1$. However, this

does not hinder practical use as F$[e_{ref}^2]$ remains close to unity up to highly eccentric orbits (e.g., for $e_{ref} = 0.99$ it takes the value 3.3566).
For the short-periodic corrections, an approximate solution is obtained as an expansion in small eccentricity. The expansion reveals that the short-periodic evolution has a sinusoidal form with high-order harmonics, showing the limitations of the numerical fitting used in [8][9]. The number of harmonics that can be captured does depend on the order of the expansion in e_{ref}. The expansions can be expressed in compact form as:

$$\begin{aligned} a_{osc}(E) &= \sum_{u=1,2,..} e_{ref}^{2u} \sum_{v=1}^{u} M_{uv}^{a} \sin 2vE \\ e_{osc}(E) &= \sum_{u=1,2,..} e_{ref}^{u-1} \sum_{v=1}^{u} M_{uv}^{e} \sin vE \end{aligned} \tag{7}$$

with coefficient matrices up to order 8 in eccentricity:

$$M^a = a_{ref} \begin{bmatrix} -1/4 & 0 & 0 & 0 \\ -1/16 & -1/128 & 0 & 0 \\ -15/512 & -3/512 & -1/1536 & 0 \\ -35/2048 & -35/8192 & -5/6144 & -5/65536 \end{bmatrix} \tag{8}$$

$$M^e = \begin{bmatrix} 2 & 0 & 0 & 0 & 0 & 0 & 0 & 0 \\ 0 & -\frac{1}{2} & 0 & 0 & 0 & 0 & 0 & 0 \\ -\frac{5}{4} & 0 & \frac{1}{12} & 0 & 0 & 0 & 0 & 0 \\ 0 & \frac{1}{4} & 0 & -\frac{1}{32} & 0 & 0 & 0 & 0 \\ -\frac{9}{32} & 0 & -\frac{1}{192} & 0 & \frac{3}{320} & 0 & 0 & 0 \\ 0 & \frac{19}{256} & 0 & -\frac{1}{256} & 0 & -\frac{1}{256} & 0 & 0 \\ -\frac{65}{512} & 0 & -\frac{5}{512} & 0 & \frac{11}{2560} & 0 & \frac{5}{3584} & 0 \\ 0 & \frac{5}{128} & 0 & \frac{1}{1024} & 0 & -\frac{1}{384} & 0 & -\frac{5}{8192} \\ -\frac{595}{8192} & 0 & -\frac{35}{4096} & 0 & \frac{7}{4096} & 0 & \frac{155}{144688} & 0 \end{bmatrix} \tag{9}$$

The semimajor axis only presents even harmonics, which differs from the assumption in [8][9] where only the first odd harmonic was considered. Instead, eccentricity presents both even and odd harmonics alternating.
The reference values for semimajor axis and eccentricity correspond to their values for $E = 0$, as follows from Eqs. (5)-(7). In general, they will differ from the initial values as the CAM will not necessarily begin at the pericentre. The a_{ref} and e_{ref} for an arbitrary initial condition (E_0, a_0, e_0) can be retrieved solving the system of 2 implicit equations:

$$a\left(E_0; a_{ref}, e_{ref}\right) = a_0 \qquad e\left(E_0; a_{ref}, e_{ref}\right) = e_0 \tag{10}$$

This system can be solved with any root finding algorithm for systems of non-linear equations. However, given that the initial and reference values are usually close (the maximum separation being the amplitude of the short periodic oscillations), in this work a fixed-point iteration was used with $a_{ref}^0 = a_0$, $e_{ref}^0 = e_0$, and the following update expression for the k-th iteration:

$$\begin{aligned} a_{ref}^k &= a_0 - \varepsilon a_{mean}\left(E_0; a_{ref}^{k-1}, e_{ref}^{k-1}\right) - \varepsilon a_{osc}(E_0; a_{ref}^{k-1}, e_{ref}^{k-1}) \\ e_{ref}^k &= e_0 - \varepsilon e_{mean}\left(E_0; a_{ref}^{k-1}, e_{ref}^{k-1}\right) - \varepsilon e_{osc}(E_0; a_{ref}^{k-1}, e_{ref}^{k-1}) \end{aligned} \tag{11}$$

Using these results, the time law in eccentric anomaly can be reduced to a root finding problem. Substituting the solutions for semimajor axis and eccentricity in terms of eccentric anomaly into Eq. (2), rearranging terms and taking the integral the time law can be expressed as:

$$\Delta t = \int_{E_0}^{E} \sqrt{\frac{a^3(E)}{\mu}} \left(1 - e(E)\cos E\right) \mathrm{d}E \tag{12}$$

It is not feasible to obtain an analytic expression for the integral using the full expressions for $a(E)$ and $e(E)$, Eq. (4). Instead, the series solution in Eqs. (5)-(9) is used. Substituting the previous expressions, expanding in power series of ε and e_{ref} (except the complete elliptic integrals inside K_a and K_e) and integrating, an approximate explicit solution is reached. The solution up to first order in ε and fourth order in e_{ref} is reported below:

$$\begin{aligned} \Delta t\, n_{ref} &= E - e_{ref} \sin E \\ &+ \varepsilon \left[E^2 \frac{3}{4} \frac{K_a}{a_{ref}} - E \left(K_e + \frac{3}{2} e_{ref} \frac{K_a}{a_{ref}} \right) \sin E + \sum_{u=1,..} e_{ref}^{u-1} \sum_{v=1}^{u} M_{uv}^E \cos vE \right] \Bigg|_{E_0}^{E} \end{aligned} \tag{13}$$

$$M^E = \begin{bmatrix} -K_e & 1/2 & 0 & 0 & 0 & 0 \\ -\dfrac{3 + 18K_a/a_{ref}}{12} & 0 & 1/12 & 0 & 0 & 0 \\ 0 & -5/48 & 0 & 1/96 & 0 & 0 \\ -1/16 & 0 & -5/192 & 0 & -1/320 & 0 \\ 0 & -19/768 & 0 & 53/15360 & 0 & 1/1280 \end{bmatrix} \tag{14}$$

Using this expression, finding the angular position for the end of the thrust arc is reduced to a root finding problem. The mean anomaly can then be computed directly through Kepler's equation, using the previous expressions for $a(E)$ and $e(E)$.

The approximate analytical solution in Eqs. (5)-(9) provides a very accurate approximation of the full numerical integration of Eq. (4), up to significant values of eccentricity. Figure 1 shows the root-mean-square error (RMSE) over 10 periods of the analytical approximation for a and e, for different values of thrust and initial eccentricity. In all cases, the initial semimajor axis is 7500 km, and the initial eccentric anomaly is 0 deg. The time law defined in differential form in Eq. (2) is also accurately represented by the analytical model, Eq. (11), as shown in Figure 2.

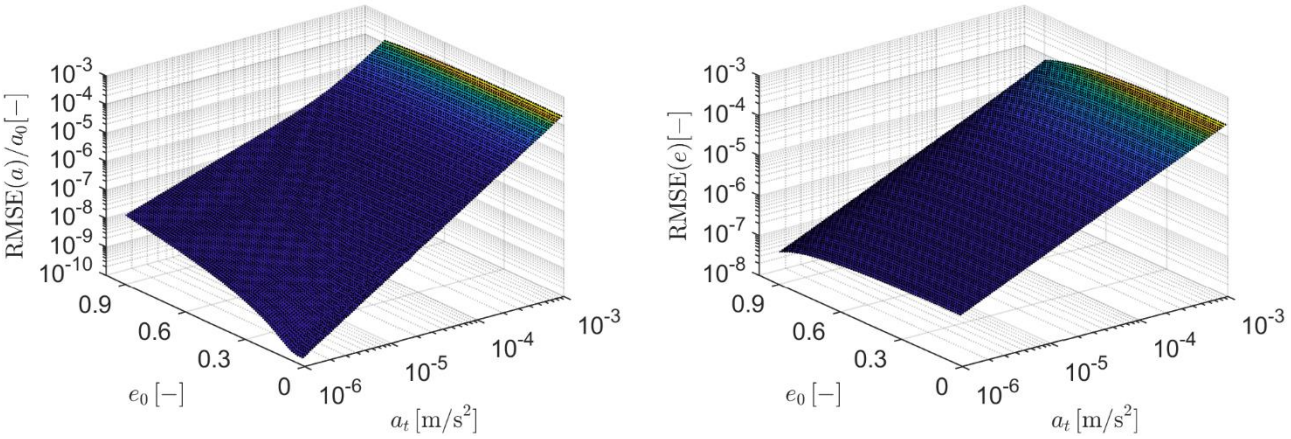

Figure 1. RMSE in 10 revolutions between the numerical (exact) and analytical (approximate) solutions, for semimajor axis (left) and eccentricity (right)

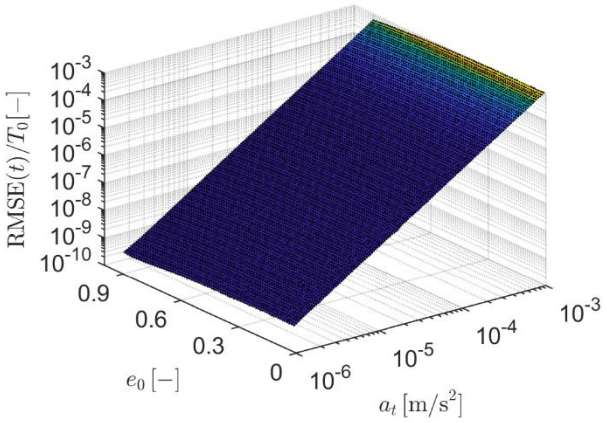

Figure 2. RMSE of the analytical time law after 10 revolutions

However, this time law is itself an approximation, obtained by taking the time derivative of Kepler's equation under the assumption of constant a and e. This simplification was made to obtain a tractable expression for the change of independent variable from time to eccentric anomaly, enabling the averaging procedure presented before. But it also poses a limitation to the practical applicability of the analytic solution, as the problem being solved separates from the actual dynamics. Because this source of error is associated to the simplifications in the differential equations of motion, it cannot be addressed by increasing the order of the expansions for a, e, and Δt. To assess the accuracy of this time law, Figure 3(a) shows the RMSE between the exact and approximate time laws $E(t)$, over 10 revolutions. Same as before, $a_0 = 7500$ km, $E_0 = 0$ deg, and $t_0 = 0$ s. The reference solution is obtained by integrating numerically the subset of differential equations for a, e, f and E in Eq. (1), while the approximate one comes from the integration of Eq. (2) together with the equations for a and e in Eq. (3). The error between the exact and approximate time laws turns out to be relatively small, but higher than those of the analytical solution. In other words, the accuracy of the CAM model would be limited by the approximate time law, rather that the use of single-averaged, analytical solutions for a, e, and $E(t)$. By comparing Eq. (2) and Eq. (1), the main missing term in the approximate time law is identified as the one due to the rotation of the line of apses under the effect of the perturbation. This was expected, as the approximate time law is derived from Kepler's law, which does not include the argument of pericentre. This suggests performing a correction of the approximate time law by adding the rotation of the line of apses. The outcome of this correction is

shown in Figure 3(b), where ω has been computed integrating numerically the corresponding of Eq. (3). This correction has reduced the RMSE, particularly for cases with larger thrust acceleration and smaller eccentricity. The latter is due to the fact that the line of apses becomes more easily affected by perturbations as the orbit approaches the circular case.

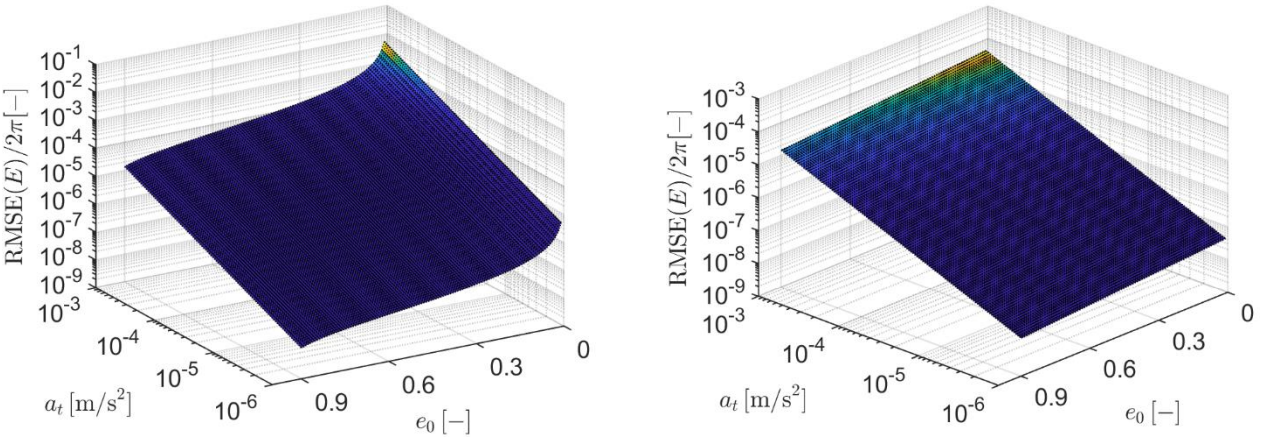

(a) for nominal time law (b) for time law with apse line correction

Figure 3. RMSE of the approximate time law $E(t)$ over 10 revolutions.

With the line of apses correction, the errors due to the time law approximation become comparable to the ones of the analytical solution. To include this correction in the computation of the CAM with the analytical model, a new expression for the change in ω is required. The differential equation for ω is symmetric in eccentric anomaly, so the mean evolution of ω will be zero. Introducing the non-dimensional thrust parameter, neglecting terms of order ε^2, assuming constant eccentricity over one revolution, and integrating, the short periodic oscillations are obtained:

$$\Delta\omega = \varepsilon \frac{2\sqrt{1-e_{ref}^2}}{e_{ref}^2}\left(2\,\mathrm{asin}\sqrt{\frac{1-e_{ref}\cos E}{2}} - \sqrt{1-e_{ref}^2\cos^2 E}\right)\Bigg|_{E_0}^{E} \tag{15}$$

The performance of the analytical solution is now compared to the semi analytical model presented in [8][9]. As already mentioned, the semi analytical solution required three numerical integrations: 1) of a and e, Eq. (3), over one period, to perform the fitting of the short-periodic corrections; 2) of the time law Eq. (2) over the complete time span of the CAM, to determine the final eccentric anomaly of the manoeuvre; 3) of the differential equation for mean anomaly in Eq. (3), over the last, incomplete revolution before the end of the thrust arc, to determine the deviation due to short-periodic oscillations. Interestingly, this last numerical integration does capture the effect of the rotation of the line of apses, so the semi analytical solution did not require the correction of $\Delta\omega$. In comparison, the new model only requires the numerical solution of the implicit time law, Eq. (13). To compare both solutions, an experimental setup like the one proposed in [8][9] is applied. Given a nominal CA involving a spacecraft and a debris, the spacecraft performs a CAM composed of a single thrusting arc of duration Δt_{CAM} and constant tangential acceleration magnitude a_t, followed by a coasting arc of duration Δt_{coast} up to the TCA. The change in Keplerian elements is evaluated using either the semi analytical (see [8][9]) or the analytical models, and it is then mapped into a displacement in the b-plane using a linearized relative motion model as described in Section 2.

Table 1. Orbital elements of spacecraft and debris at CA, for test cases A and B

Case	Object	a [km]	e [−]	i [deg]	Ω [deg]	ω [deg]	f_0 [deg]
A	PROBA-2	7093.637	0.00146	98.244	303.595	109.499	179.499
	Debris	7782.193	0.08716	88.690	142.727	248.168	1.223
B	Molniya 2-9	23236.962	0.66819	64.209	286.999	285.583	14.043
	Debris	12962.638	0.31805	84.017	286.871	282.796	76.864

Two test cases are considered, reported in Table 1. Case A is the same one presented in [8][9], and it is revisited using both the former semi analytical method and the new fully analytical method. This test case corresponds to a CA between PROBA-2 and a virtual debris constructed statistically using data from MASTER-2009. Figure 4 shows the displacement in the b-plane δb for different values of a_t and Δt_{CAM}, and a fixed coast arc duration of 3 nominal periods of the spacecraft. Additionally, Figure 4(c) and Figure 4(d) provide a quantitative measure of the error of both methods, using a numerical integration of Eqs. (3) along the thrust arc as reference solution.

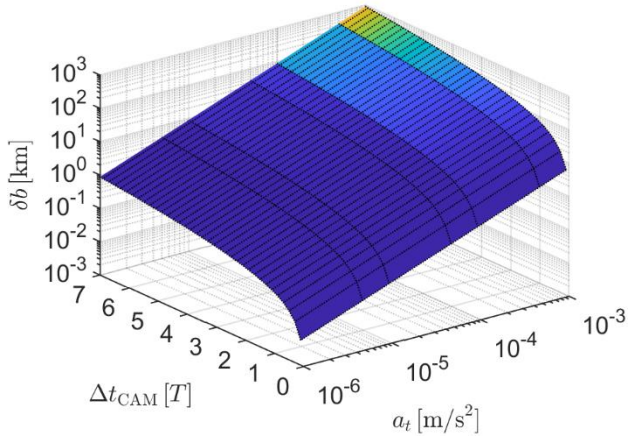

(a) δb, analytical method

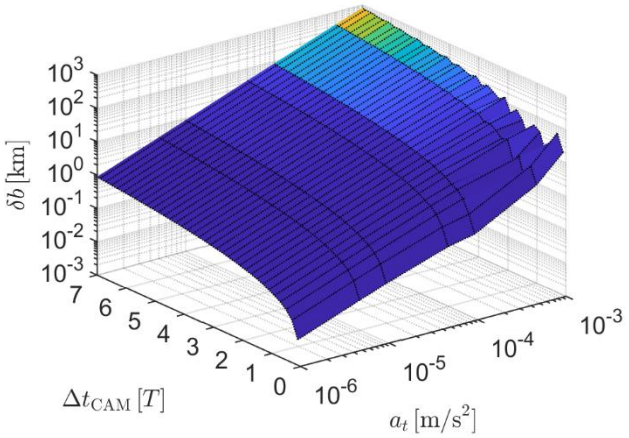

(b) δb, semi analytical method

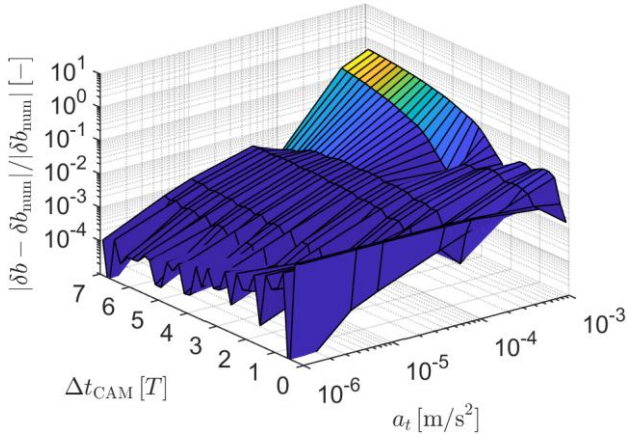

(c) Error in δb, analytical method

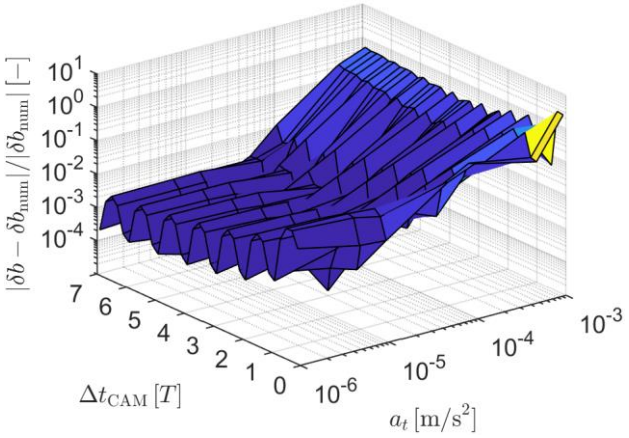

(d) Error in δb, semi analytical method

Figure 4. Displacements in the b-plane and relative errors for Case A and a $\Delta t_f = 3T$, both for the analytical (left) and semi analytical (right) models

The results show that the analytical method improves the behaviour of the model for relatively high values of thrust acceleration, no longer showing irregular patterns for accelerations close to $0.001\ \mathrm{m/s^2}$. This is further confirmed by the error plots. One key difference supporting the better behaviour of the analytical model is that it captures the frequencies of the short-periodic corrections better than the sinusoidal fitting in the semi analytical model. Particularly, while the dominant harmonic of eccentricity has indeed period 2π, the first harmonic for a is already 4π. This was not adequately captured by the sinusoidal fitting, leading to significant errors as the amplitude of the oscillations grew with a_t.

Test case B corresponds to a high-eccentricity object, classified in Space-Track [14] as "Molniya 2-9" (NORAD ID 7276). The Keplerian elements for the spacecraft are retrieved from [14] at epoch 2021-05-09, 17:32:21, while the debris has been generated setting a random relative velocity at CA. The resulting displacements and relative errors for a fixed $a_t = 10^{-6}\ \mathrm{m/s^2}$ and different values of Δt_{CAM} and Δt_f are represented in Figure 5. Because the orbital period is now larger, a shorter number of periods for the thrust and coast arcs are needed to get significant displacements. But more interestingly, the analytical solution captures several oscillatory patterns that were lost in the semi analytical one. These patterns are due to the different effect of thrusting close to the pericentre or the apocentre, and are also present in the exact numerical solution (not included here for brevity).

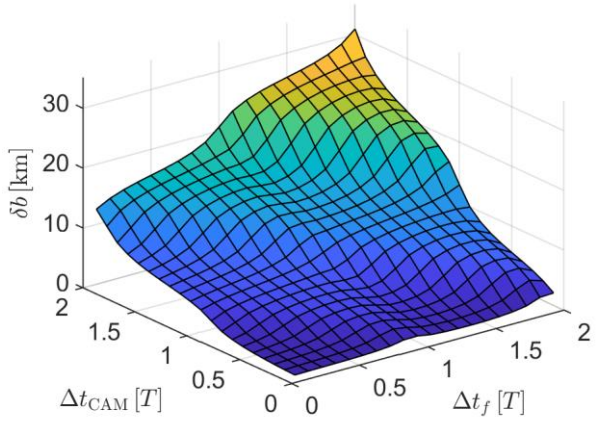

(a) δb, analytical method

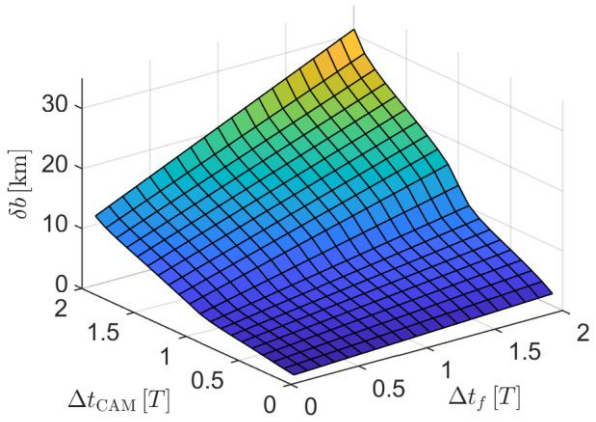

(b) δb, semi analytical method

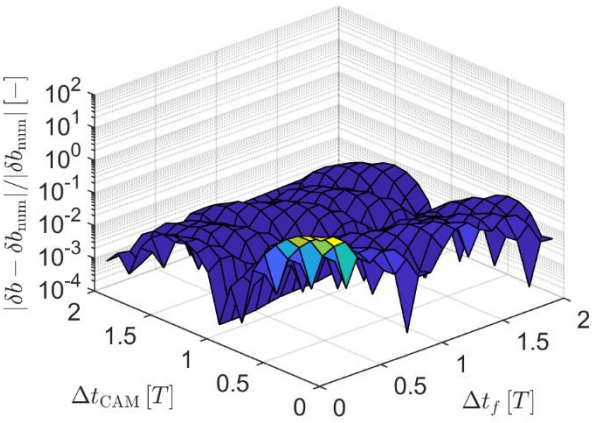

(c) Error in δb, analytical method

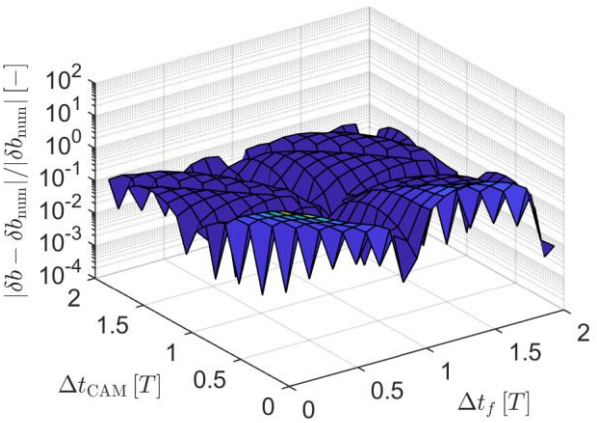

(d) Error in δb, semi analytical method

Figure 5. Displacements in the b-plane and relative errors for Case B and $a_t = 10^{-6}\ \mathrm{m/s^2}$, both for the analytical (left) and semi analytical (right) models

Table 2 summarizes the computational costs for each test case and model. Each case was evaluated over a 3D grid of $(a_t, \Delta t_{CAM}, \Delta t_f)$, with 7 values of a_t logarithmically spaced between 10^{-3} m/s^2 and 10^{-6} m/s^2, 100 values of Δt_{CAM} uniformly spaced between 0 and 10 periods of the nominal spacecraft orbit, and 100 values of Δt_f distributed in the same way as Δt_{CAM}. The tests were executed on an Intel Core i7-8700 CPU @3.20 GHz running Matlab 2020b, and the code for all the three methods was compiled with Matlab Coder to avoid overheads. The analytical method clearly outperforms the other 2, being one order of magnitude faster than the reference numerical solution. It is also observed that the high eccentricity case is significantly more costly to solve, being the semi analytical and numerical methods, in that order, the most affected in relative terms.

Table 2. Computational times for different test cases and models

Test case	**Computational time [s]**		
	Numerical	**Semi analytical**	**Analytical**
Case A	105.793588	32.704746	1.559827
Case B	346.827833	158.348271	2.003455

4 STM INCLUDING DRAG and SOLAR RADIATION PRESSURE

The analytical model in Section 3 only includes thrust acceleration as perturbation. This is a reasonable approximation for short manoeuvre times when thrust is the dominant perturbation, but there are scenarios where other perturbations can become relevant. A practical example are CAMs performed by spacecraft deorbiting through drag-augmentation devices such as sails [15]. In [3], the capability of sail-equipped deorbiting spacecraft to perform CAMs was evaluated, considering a simple on/off control law for the sail orientation and propagating the trajectory numerically with PlanODyn [10]. PlanODyn is a semi analytical propagator, that numerically integrates the single-averaged equations of motion in Keplerian elements. While effective, this approach has two main limitations: a high computational cost if multiple design parameters are considered, and limited insight on how each parameter affects the displacement in the b-plane.

To address these issues, PlanODyn capabilities have been extended to compute STMs that retain the effect of drag- and SRP-related parameters. This involved two main steps:

1. An extended state vector was defined as $\boldsymbol{\alpha}^* = [\,\boldsymbol{\alpha}; \boldsymbol{\beta}]$ with $\boldsymbol{\beta} = [c_D;\ (A/m)_D;\ c_R;\ (A/m)_R]$, where c_D is the drag coefficient, $(A/m)_D$ is the area-to-mass ratio for drag, c_R is the reflectivity coefficient, and $(A/m)_R$ is the area-to-mass ratio for SRP. Note that both A/m are kept separate so it is possible to account for different attitudes of the spacecraft. The drag- and SRP-related states are assumed to be constant during the propagation, so the differential equations for the new states are equal to 0. Further extensions could be possible by defining them as functions of time and the state.
2. The variational equations for the STM $\boldsymbol{\Phi}(t; t_0)$ were added to the equations of motion, to be integrated simultaneously with the extended state. The variational equations are given by:

$$\dot{\boldsymbol{\Phi}}(t; t_0) = \boldsymbol{J}^*(t)\boldsymbol{\Phi}(t; t_0) \tag{16}$$

with $\boldsymbol{\Phi}(t_0; t_0) = \boldsymbol{I}$, where $\boldsymbol{J}^*(t)$ is the Jacobian of the equations of motion for the extended state $\boldsymbol{\alpha}^*$, and the STM for the extended state vector $\boldsymbol{\alpha}^*$ has dimensions 10×10. Together with the equations of motion, they define a system of 110 ordinary differential equations.

The Jacobian $\boldsymbol{J}^*$ can be conveniently expressed in block form as follows:

$$\boldsymbol{J}^* = \begin{bmatrix} \boldsymbol{J} & \boldsymbol{K} \\ \mathbf{0}_{4\times 6} & \mathbf{0}_{4\times 4} \end{bmatrix} \tag{17}$$

where $\boldsymbol{J}$ is the Jacobian corresponding to the original state vector $\boldsymbol{\alpha}$, $\boldsymbol{K}$ is a 6×4 matrix containing the partial derivatives of the equations of motion with respect to $\boldsymbol{\beta}$, and $\mathbf{0}_{u\times v}$ is a $u \times v$ zero matrix. Note that, since drag and SRP acceleration depend linearly on their corresponding coefficient and area-to-mass, the components of $\boldsymbol{K}$ can be computed simply by division.

From Eq. (17), it follows that the Jacobian for each perturbation force model is needed in order to compose the full Jacobian $\boldsymbol{J}^*$. The following perturbation force models have been used, all of which have an analytical implementation for the Jacobian of the single-averaged equations of motion:

- Non-spherical gravity field: only J_2 is considered.
- Atmospheric drag: an extension of King-Hele's contraction method by Frey et al. [16], for application in semi analytical propagation.
- SRP: Cannonball model without eclipses.

Taking $t = t_{CA}$, the STM relates changes in the orbit at t_0 with changes in the orbit at t_{CA} as $\delta\boldsymbol{\alpha}^*(t_{CA}) = \boldsymbol{\Phi}(t_{CA}; t_0)\delta\boldsymbol{\alpha}^*(t_0)$. This structure is analogous to other models for orbit modification in MISS, so it can be used together with the relative motion equations and the b-plane projection to carry out analyses like the one for the impulsive CAM in [2]. However, in this case we will have $\delta\boldsymbol{\alpha}(t_0) = \mathbf{0}$, and $\delta\boldsymbol{\beta}(t_{CA})$ is not needed for the evaluation of the displacement. Therefore, calling $\widehat{\boldsymbol{\Phi}}$ to the 6×4 upper-right submatrix of $\boldsymbol{\Phi}(t_{CA}; t_0)$ and multiplying by the relative motion matrix and the b-plane projection matrix one finally reaches:

$$\delta\boldsymbol{b}(t_{CA}) = \boldsymbol{M}_{\delta b}\boldsymbol{A}_r\, \widehat{\boldsymbol{\Phi}}\, \delta\boldsymbol{\beta}(t_0) \tag{18}$$

where $\boldsymbol{A}_r$ is the part of relative motion matrix $\boldsymbol{A}$ related to the displacement, and $\boldsymbol{M}_{\delta b}$ gives the projection of a position vector onto the b-plane [2][9]. Note that the second component in $\delta\boldsymbol{b}$ is normal to the encounter plane, and does not contribute to modifying the miss distance.

To conclude this section, an application example is presented. Let us consider the nominal CA between a sail-equipped deorbiting satellite and a debris summarized in Table 3. The spacecraft has fixed values for $c_D = 2.1$, $c_R = 1.0$ and $(A/m)_R = 0.5\,\mathrm{m}^2/\mathrm{kg}$. The nominal value for $(A/m)_D$ during the deorbiting phase is also $0.5\,\mathrm{m}^2/\mathrm{kg}$, but the spacecraft is capable of controlling it in the range $(A/m)_D \in [0.4\ 0.5]\,\mathrm{m}^2/\mathrm{kg}$. To avoid the debris, the spacecraft changes its drag area-to-mass by an amount ΔD during an arc of duration Δt before the TCA. The resulting deviation inside the b-plane and the error with respect to an exact reference solution are depicted in Figure 6, where the compounded effects of lead time and drag modification can be observed. One numerical propagation with PlanODyn is required for each Δt to evaluate the STM, but then the results for all the ΔD are evaluated through a matrix-vector multiplication. Finally, the STM is, by definition, a linearization. Therefore, the validity of the solution is limited to small values of ΔD as shown in the error plot.

Table 3. Orbital elements of spacecraft and debris for the sail CAM test case.

Object	$\boldsymbol{a}$ **[km]**	$\boldsymbol{e}$ **[−]**	$\boldsymbol{i}$ **[deg]**	$\boldsymbol{\Omega}$ **[deg]**	$\boldsymbol{\omega}$ **[deg]**	$\boldsymbol{f_0}$ **[deg]**
Spacecraft	7200.000	0.000252	1.003	0	0	28.648
Debris	7444.280	0.313246	137.379	29.181	258.300	102.410

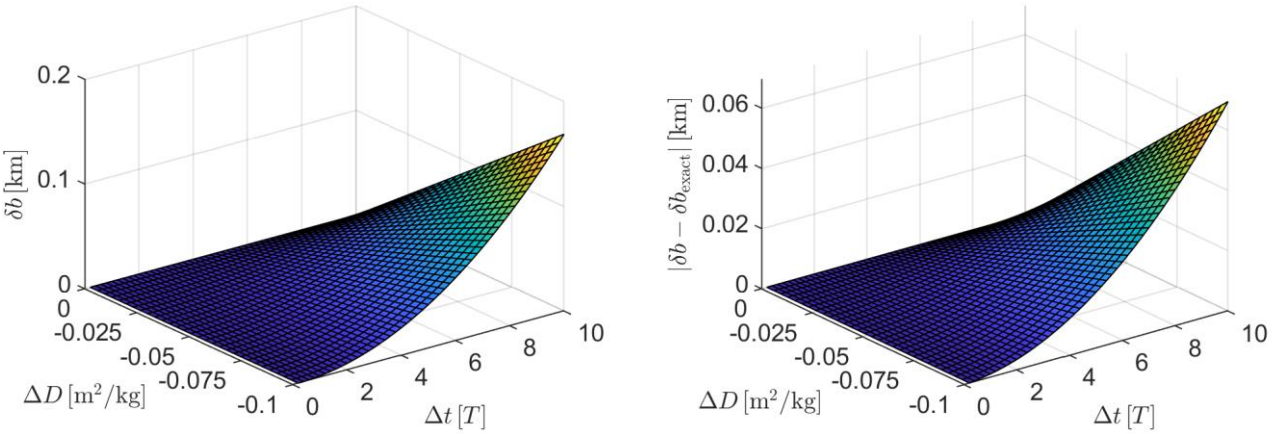

Figure 6. Results for the sail CAM: estimated deviation in the b-plane (left) and absolute error with respect to a reference solution computed numerically (right).

5 APPLICATIONS for ON-BOARD AUTONOMY

The algorithms presented in this work provide computationally cheap yet accurate ways to model CAMs. And particularly, the analytical equations for low-thrust CAM in Section 3 can be suitable for on-board implementation given their simple structure and very reduced computational cost. However, to achieve real on-board autonomy a decision-making component is needed, to determine whether the CAM is needed in the first place. This decision should be taken in a similar way to current human-driven operations, based on the evolution of the Conjunction Data Messages (CDMs) and additional navigation information from the satellite. This decision-making task can be tackled through AI and ML algorithms. A significant event in this field was the Collision Avoidance Challenge organized by ESA as part of the CREAM initiative [17]. The participants built models to estimate the final collision risk based on a dataset of real-world CDMs. The submissions were evaluated based on their capability of discriminating high risk events (collision probability greater than 10^{-6}) from low risk events, and estimating the final risk at CA of the former. A summary of the outcomes of the competition can be found in [17]. Two key conclusions are the difficulty to define a proper training set, and the need to assess the adequacy of ML algorithms for the decision-making task. The scarcity of real-world data to train the algorithm could be addressed by generating synthetic datasets, like done by Vasile et al. [18].

By combining these two elements, a framework for autonomous on-board COLA operations is defined, composed by two building blocks: a ML-powered decision-making module, and a CAM design module based on analytical models. To test this framework, an autonomous COLA experiment is proposed as part of a CubeSat demonstration mission that the COMPASS group is promoting in collaboration with several Italian partners, called e.Cube [19]. e.Cube aims at contributing to the advancement of technologies and methodologies dedicated to space debris mitigation and remediation. Three different experiments are devised: 1) implementation and validation of on-board autonomous COLA capabilities; 2) untraceable space debris in-situ detection, acquiring data to support current and future models for small debris; 3) re-entry characterization, providing direct measurements on the atmospheric conditions and the spacecraft mechanical behaviour during re-entry. The COLA experiment will consist of several in-flight CAM tests for simulated CAs with a virtual debris. The proposed experiment will use impulsive CAMs, with the analytical models in [2], but the results regarding the decision-making module will be applicable also to the low-thrust case, accounting for the additional time needed by the CAM. For each test, a sequence of CDM-like messages describing the predicted CA for different warning times is generated on ground and

uploaded to the spacecraft, and from it passed to a dedicated on-board computer called CAM Control Module (CCM). The CCM will then decide if and how to instruct the spacecraft to perform the manoeuvre, and log all the process for analysis. The outcomes of the manoeuvre will be measured through the state after manoeuvre compared with the expected one, and the change in collision probability. Of the different test cases considered, a particularly interesting one is last-minute autonomous CAM, to verify the feasibility of a spacecraft performing a CAM based on data from a federated SSA network about an impending CA that had gone previously undetected.

6 CONCLUSIONS

The latest developments in the analytical and semi analytical algorithms of the MISS suite for the modelling of CAMs have been presented, with a focus on low-thrust manoeuvres. First, a fully analytical approximate solution for constant, tangential low-thrust CAMs was developed in detail, reaching straightforward expressions depending on trigonometric functions and complete elliptic integrals of the first and second kind. Even though the analytical model is expressed as a power series of small thrust acceleration and eccentricity, the numerical test cases show that it performs well also for highly eccentric orbits and values of the acceleration beyond those typical of current electric propulsion systems. Furthermore, the analytical solution not only was faster but also more accurate than the previous semi analytical solution.

The analytical model only takes the thrust acceleration as perturbation. To deal with CAs where drag and SRP play an important role, an extension to the semi analytical, single-averaged orbit propagator PlanODyn was proposed to obtain STMs retaining the effect of the area-to-mass ratio and the drag and reflectivity coefficients. By extending the state vector to include those parameters and integrating the variational equations, a linear expression for the displacements in the b-plane at the nominal TCA due to small changes in the drag and SRP parameters is computed.

The straightforward formulation and small computational cost of the low-thrust CAM model make it suitable for potential on-board applications. However, by itself it lacks the capacity of advanced decision-making based on a series of CDMs for a predicted CA. A framework for autonomous on-board collision capabilities, part of a proposed CubeSat demonstration mission, has been presented and briefly discussed. This framework is composed of a ML-powered decision-making module, and a CAM design module using analytical models.

7 ACKNOWLEDGEMENTS

This project has received funding from the European Research Council (ERC) under the European Union's Horizon 2020 research and innovation programme (grant agreement No 679086 – COMPASS).

8 REFERENCES

[1] https://www.compass.polimi.it/

[2] Gonzalo J.L., Colombo C. and Di Lizia P., Analytical framework for space debris collision avoidance maneuver design. *Journal of Guidance, Control and Dynamics*, Vol. 44, No. 3, 469-487, 2021. https://doi.org/10.2514/1.G005398

[3] Gonzalo J.L., Colombo C. and Di Lizia P., Analysis and Design of Collision Avoidance Maneuvers for Passive De-Orbiting Missions, *2018 AAS/AIAA Astrodynamics Specialist Conference*, Snowbird (UT), 19 -23 Aug 2018. No AAS 18-357

[4] Gonzalo J.L., Colombo C. and Di Lizia P., A semi-analytical approach to low-thrust collision avoidance manoeuvre design, *70th International Astronautical Congress*, Washington, D.C., USA, 21-25 October 2019. IAC-19-A6.2.3

[5] Conway B.A., Near-optimal deflection of earth-approaching asteroids, *Journal of Guidance, Control, and Dynamics*, Vol. 24, No. 5, 1035-1037, 2001.

[6] Bombardelli C. and Hernando-Ayuso J., Optimal impulsive collision avoidance in low Earth orbit, *Journal of Guidance, Control, and Dynamics*, Vol. 38, No. 2, 217-225, 2015.

[7] Gonzalo J.L., Colombo C. and Di Lizia P., Drag- and SRP-induced effects in uncertainty evolution for close approaches, *4th KePASSA*, Logroño, Spain, 24-26 April 2019.

[8] Gonzalo J.L., Colombo C. and Di Lizia P., Introducing MISS, a new tool for collision avoidance analysis and design, *1st International Orbital Debris Conf.*, Sugarland, TX, USA, 9-12 Dec. 2019.

[9] Gonzalo J.L., Colombo C. and Di Lizia P., Introducing MISS, a new tool for collision avoidance analysis and design, *Journal of Space Safety Engineering*, Vol. 7, No. 3, 282-289, 2020. https://doi.org/10.1016/j.jsse.2020.07.010

[10] Colombo C., Planetary Orbital Dynamics (PlanODyn) suite for long term propagation in perturbed environment, *6th ICATT*, Darmstadt, Germany, 14-17 March 2016.

[11] Vasile M. and Colombo C., Optimal impact strategies for asteroid deflection, *Journal of Guidance, Control, and Dynamics*, Vol. 31, No. 4, 858–872, 2008. https://doi.org/10.2514/1.33432

[12] Huang S., Colombo C. and Bernelli-Zazzera F., Orbit raising and de-orbit for coplanar satellite constellations with low-thrust propulsion, *4th IAA Conference on Dynamics and Control of Space Systems*, Changsha, China, 21-23 May 2018. Paper IAA-AAS-DyCoSS4-1-15.

[13] Colombo C., Vasile M. and Radice, G., Semi-analytical solution for the optimal low-thrust deflection of near-Earth objects, *Journal of Guidance, Control and Dynamics*, Vol. 32, No. 3, 796-809, 2009. https://doi.org/10.2514/1.40363

[14] https://www.space-track.org

[15] Colombo C., et al, Effects of passive de-orbiting through drag and solar sails and electrodynamic tethers on the space debris environment, *69th International Astronautical Congress*, Bremen, Germany, 1-5 Oct. 2018.

[16] Frey S., Colombo C., and Lemmens S., Extension of the King-Hele orbit contraction method for accurate, semi-analytical propagation of non-circular orbits, *Advances in Space Research*, Vol. 64, No. 1, 1-17, 2019. https://doi.org/10.1016/j.asr.2019.03.016

[17] Uriot,T. et al., Spacecraft collision avoidance challenge: Design and results of a machine learning competition, *Astrodynamics*, 2021. https://doi.org/10.1007/s42064-021-0101-5

[18] Vasile M., Rodriguez-Fernandez V., Serra R., Camacho D. and Riccardi A., Artificial Intelligence in Support to Space Traffic Management, *68th International Astronautical Congress*, Adelaide, Australia, 25–29 Sep. 2017. Paper IAC–17.A6.7.1.

[19] Colombo C. et al., e.Cube mission: the Environmental CubeSat, *8th European Conference on Space Debris*, ESA/ESOC, Darmstadt, Germany, Virtual Conference, 20-23 Apr. 2021.